# An Inchworm Mobile Robot using Electromagnetic Linear Actuator

## 1. Introduction

The capability of motion is the important aspect for a micro robot to fulfill its on-board control and given tasks, and therefore the micro actuators play a key role in the micro robotic systems. Various applications of the robotic systems suggest the use of new actuator systems, which allow motion to be realized with different characteristics, such as accuracy, force, travel, etc. Micro autonomous systems usually require large force, large displacement and less power consumption. Many actuation principles have been reported in the past decades and they were mainly electrostatic [1][2][3], piezoelectric [4][5] [6] and electromagnetic [7][8][9]. The electrostatic actuator exhibits low force with very small air gap, fast response and low power consumption. However, the maximum displacement perpendicular to the electrodes is restricted and not suitable for the applications where displacements are larger than several micrometers. Piezoelectric actuator, on the other hand, provides sufficiently high output force with large gap and good response. Whereas, the actuator displacement is also severely limited and a high driven voltage (tens to hundreds of volts) is usually required. Electromagnetic actuator features moderate output force, large displacement and can be driven by common low cost, low voltage controller. Although they were difficult in the fabrication and miniaturization of complicated electromagnetic structures, with the recent development in nano-magnetic materials and micro machining technology [10], it is no longer a problem to extend them to the micro applications.

Although different actuation principles have their advantages and drawbacks, the application of these principles is also a challenge. Many actuation mechanism using different principles have been developed to meet various robotic applications [11] [12] [13]. Among those researched, inchworm robot is a compact design option that generates the large displacement with necessary output force. An inchworm robot imitates the locomotion pattern of a natural inchworm. Generally, it consists of two main components: an actuating module that can deform in the direction of travel and a mechanism that produces friction against the environment, such as grippers. The motion of the robot is realized by repeating a clamp-extend-clamp cycle through a series of actuator actions [14]. This kind of robots are especially useful in traveling and conducting tasks in narrow and highly constrained environments, such as pipes and conduits in industrial plants, or slender vessels and intestines in human body [15].

A commonly used elongation actuator in an inchworm robot is made from lead zirconate titanate (PZT) material. It performs a quick expansion and contraction by energizing and de-energizing the PZT elements. A typical PZT based inchworm actuator is show in Fig.1 (a) [16]. As mentioned before, a powerful voltage supply is necessary for the operation of such piezo actuator. An alternative option is the electromagnetic actuator. One of the designs is utilizing the stick-slip principle by controlling the electromagnetic force between a solenoid and a permanent magnet (PM). A reported example is illustrated in Fig.1 (b) [17]. Although the driven force of an electromagnetic inchworm actuator is usually less than that of a PZT type counterpart, the travel stroke of electromagnetic inchworm actuator is much larger. Moreover, the electromagnetic actuator is a current source driven device that could be operated at low voltages. Therefore, batteries or wireless power supply is possible with the electromagnetic actuators.

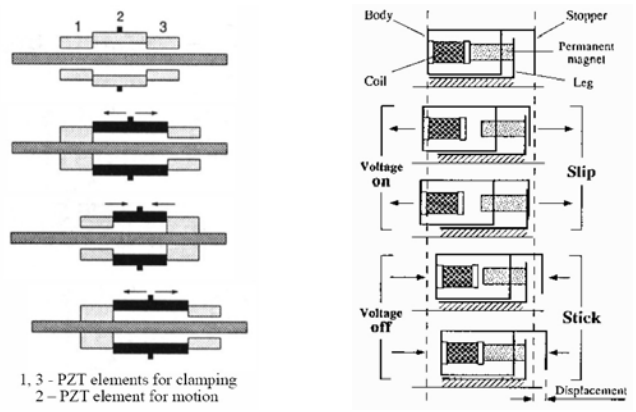


(a) (b)

Fig.1 Examples of inchworm robot (a) PZT-based, (b) electromagnetic

A frictional clamping mechanism is usually required for the motion of the inchworm robot. A PZT-based clamping element is used in the design shown in Fig.1 (a). In addition, electromagnet can also be used for the attachment of the robot to the travel surface [18]. However, this type of friction generation is effective only on the ferrite surface. Another effectual design imitates the function of the scales of a worm or snake, which can have anisotropic frictional forces when contacting with the ground. An example is shown in Fig.1 (b) that a unidirectional movement is achieved by the artificial bristles mounted under the autonomous robot.

In this paper, a bristle-based inchworm mobile robot by using a short stroke electromagnetic linear actuator is presented. The actuator is made up of thin amorphous soft magnetic ribbon and high energy product PMs. The structure of the actuator was deliberately designed to achieve optimal output force and necessary travel stroke within the limited dimensions. A large and an actual scaled prototype were constructed for the performance verification. In order to investigate the dynamic performances of the mobile robot, a comprehensive model was built according to the characteristics of the actuator and mechanics of the robotic system. In addition, a novel drive scheme for the proposed linear actuator was developed for the motion control of the robot.

## 2. Mobile Robot Design

Fig.2 shows the schematic structure of the proposed mobile robot. It consists of a tubular main body and two bristle-like legs or fins. A tubular type electromagnetic linear actuator is installed within the main body. The stator of the actuator is attached to the main body and the mover of the actuator acts as a movable unit of the robot that can make the robot extend or contract. The front leg or fin is attached to the main body while the other is attached to the movable unit. A bellows seal is employed between the main body and the movable units so that the robot can operate in liquid environment. A spring is installed either inside or outside the actuator between the stator and mover for the restoration of the starting position of the mover. The elastic coefficient of the spring is deliberately designed to generate force at full stroke equal to the electromagnetic force of the linear actuator. The application of the spring could also reduce the power consumption of the actuator. The legs of the robot are made by single leaf springs and are tilted with a pre-adjusted angle so that they can provide unidirectional movement. Meanwhile, they can function as fins when traveling in liquid.

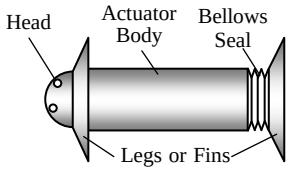


Fig.2 Schematic structure of the inchworm robot

The operation principle is shown in Fig.3. During the locomotion cycle, an electromagnetic force will be generated to make the mover shift forward from its starting position (Fig.3 (a) and (b)). When the mover reaches maximum allowable stroke, the electromagnetic force is removed. The main body will go forward due to the force of the spring installed (Fig.3 (c)) and the mover will restore its relative starting position for the next locomotion cycle (Fig.3 (d)). During the operation, the self-lock mechanism of the legs can prevent the components from sliding backward.

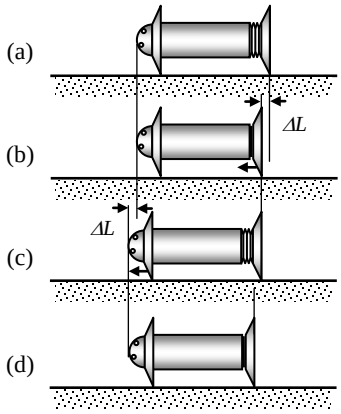


Fig.3 Operation of the proposed inchworm robot

## 3. Electromagnetic Linear Actuator

### 3.1 Basic Structure

Fig.4 shows the basic configuration of the tubular linear PM actuator for the inchworm robot and the elementary dimensions of the actuator are listed in Table I. The external diameter of the actuator is about 7mm and total length of the actuator is approximately 10mm. The stator core and the pole-pieces of the mover are made up of glassy metal ribbon, which features very high magnetic permeability and extremely low core loss. The mover is assembled by putting the PMs and the pole-pieces alternately along the shaft, as shown in Fig.4. The amount of the PMs is determined based on the tradeoff between the flux density and the saturation of the magnetic core [19]. All the non-magnetic components of the actuator are made from aluminum for the reduction of the volume of the PM material and the entire moving mass [20]. A number of circular coils are mounted inside the stator and are uniformly grouped into three phases.

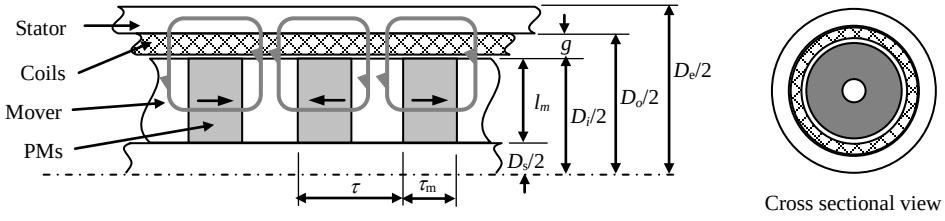


Fig.4 Configuration of the linear actuator

TABLE I
Elementary Dimensions of the Actuator

| | |
|---|---|
| Outer Diameter of Stator | $D_e$ |
| Inner Diameter of Stator | $D_o$ |
| Stator Length | $L_e$ |
| Gap between Stator and Mover | $g$ |
| Mover Diameter | $D_i$ |
| Mover Length | $L_a$ |
| Thickness of PM Disc | $\tau_m$ |
| Pole Pitch | $\tau$ |
| Mover Shaft Diameter | $D_s$ |

3.2 Optimal Design of the Force Output

According to Lenz's law, it can be derived that the electromagnetic force generated by the current in the coils of the actuator is

$$F_{em} = p\phi_g J_s h_c l_c , \qquad (1)$$

where $\phi_g$ is the magnetic flux in the air gap of the actuator, $p$ the number of poles, $J_s$ the current density in the coils, and $h_c$, $d_c$ and $l_c$ are the height, effective width and mean perimeter of the coils under one pole, respectively. Hence, an optimal force output can be achieved by appropriate design of $\phi_g$ and inner diameter of the actuator that makes the best of the actuator volume. Via magnetic field analysis, it can be found that the magnetic flux in the air gap will be maximum when $\tau = 2\tau_m$ [21].

Based on the results, the electromagnetic force of the actuator can be further obtained as

$$F_{em} = \mu_0 \pi p H_c J_s k_f \frac{\tau^2 l_m (D - l_m)(D_s + l_m)(D + D_s + l_m)}{16 l_m (D - l_m)(D_s + l_m) + \tau^2 (D + D_s + l_m)}, \qquad (2)$$

where $H_c$ is the coercive force of the PM, $k_f$ the fill factor of the coils, $l_m = (D_i - D_s)/2$ is the radial width of the PM disc, and $D = (D_o - D_s)/2$ the space between the stator core and mover shaft.

For a given volume of the actuator, $D$ and $\tau$ will be fixed. Consequently, $F_{em}$ will vary with the radial width of the PM discs $l_m$. In order to get the appropriate value of $l_m$, the variation of $F_{em}$ versus the ratio of $l_m/D$ is analyzed based on the proposed dimensions and the results are plotted in Fig.5 (a). It can be seen that there exists an optimal ratio of $l_m/D$, which gives a maximum force output. From the formulation, it can be found that this optimal ratio is 0.78 and then the diameter of the mover $D_i$ could be set. A finite element (FE) magnetic filed analysis was performed for the verification and the computed results are shown in Fig.5 (b).

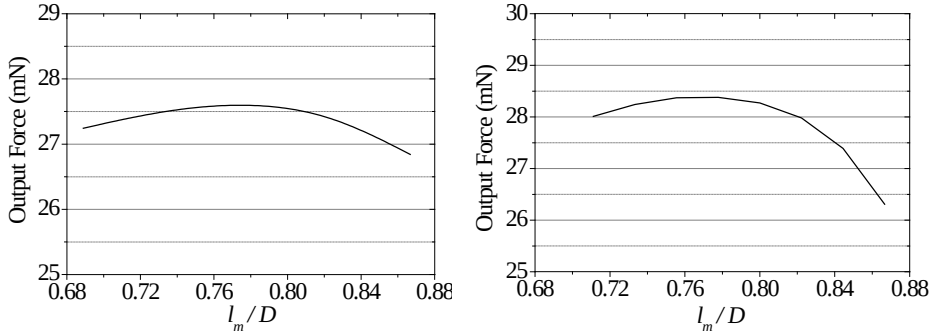


(a) (b)

Fig.5 Output force (a) Analytical result; (b) FE analysis result

3.3 Electromagnetic Force of the Actuator

By applying the dimensions obtained above, the electromagnetic force throughout the entire stroke of the actuator was analyzed. Since the mover of the actuator is deliberately designed shorter than the stator so that it can move back and forth within the stator, the distribution of the resultant flux density in the air gap varies with the position of the mover and so does the produced electromagnetic force. In addition, due to the limited length of the actuator, the flux density and force when the armature is close to the extremities of the stator core will differ from those when the mover is in the middle of the actuator.

The excitation scheme for the proposed actuator is the brushless DC drive method. The brushless DC drives are widely used in the PM machines due to their simple implementation and very good control performance. Moreover, a brushless DC drive without the mechanical position sensor can be easily realized by the phase voltage detection. These features are very attractive for the cost-effective miniature systems that do not allow complex system structure and large volume.

The excitations of the brushless DC drive are the direct currents imposed to the stator windings of the actuator according to the mover positions. Normally, the 120˚ square wave energization (Fig.6) is employed for the three-phase machine. The winding currents are required to be commutated at the proper mover positions to achieve the optimal force output.

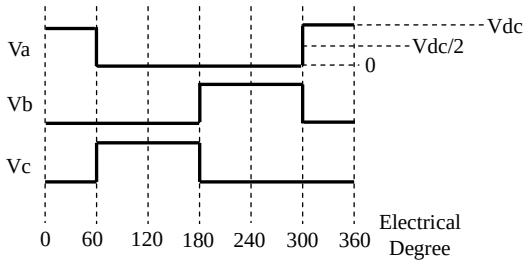


Fig.6 120˚ square wave energization

Based on the excitation principle, the electromagnetic force of the actuator was computed at different mover positions by the FE analysis. The amplitude of the winding current is determined by the permissible current density limited by the thermal condition. A proper switching sequence as well as a set of commutation positions was found by comparing the forces at different mover positions. The calculated electromagnetic force, which is obtained by the acquired brushless DC excitation sequence and optimal commutation positions listed in Table II, is shown in Fig.7.

TABLE II

| | Energization Sequence | | | |
|---|---|---|---|---|
| Stroke | 0 – 13.3% | 13.3 – 50% | 50 – 86.7% | 86.7 – 100% |
| Energization | $A\overline{B}$ | $\overline{B}C$ | $\overline{A}C$ | $\overline{A}B$ |

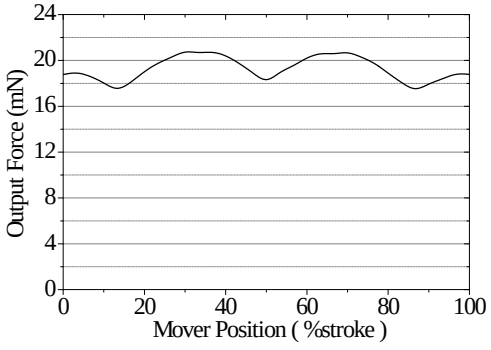


Fig.7 Force of the actual sized actuator

3.4 Prototype Construction

Two prototypes with different scales were constructed for the performance verification. One prototype is the desired size and the other is five times bigger. The stator tubes for the prototypes are shown in Fig.8. The stator windings were made up of single annular coils shown in Fig.9. They were mounted between the stator and mover and connected as required for the appreciate control scheme.

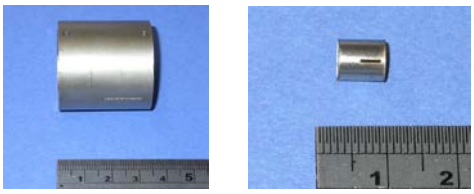

Fig.8 Stator core for the different sized prototypes

Fig.9 Stator coils for the different sized prototypes

The pole-pieces used on the mover were stacked by the glassy metal sheets that were cut into the required shape in advance. The mover was then constructed by assembling the pole-pieces and the PM discs alternatively along the shaft, as shown in Fig.10. Fig.11 shows the photographs of the completed prototypes.

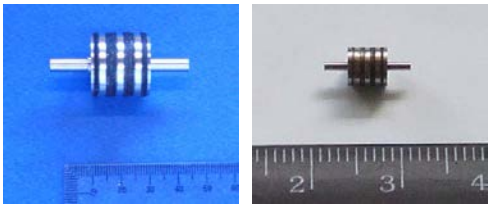

Fig.10 Assembled movers

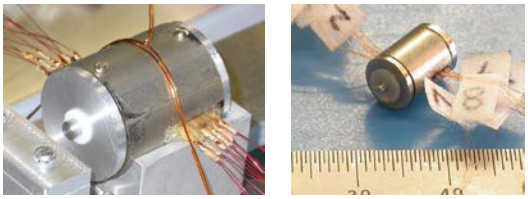

Fig.11 Completed prototypes

3.5 Experimental Verification

A comprehensive experiment was carried out on the prototype to verify the performance of the proposed actuator. A precision test bench was designed for the prototype testing. As shown in Fig.12, the test bench consists of a force gauge, a micro position meter, a tool set for clamping the actuator being tested, and a supporting stage. The position of the mover was preset by the micrometer before the measurement of the actuation force. In addition to the forces, the test bench was also used for the measurement of the phase inductances at different mover positions.

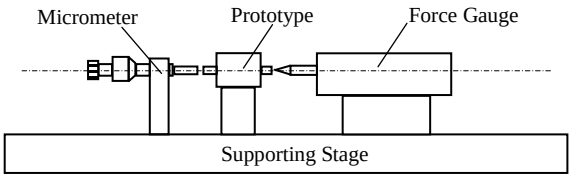


Fig.12 Test bench for the prototype

During the measurement, a DC current was fed into to the actuator according to the energization sequence shown in Table II. The amplitude of the current was set to meet the current density used for the previous analysis. Fig.13 shows the measured force of the large-scaled prototype together with the predicted results as a comparison. It can be seen that the predicted forces agree well with the measurement. Compare with the analyzed output force of the small-sized actuator, the results meet the cubic scale effect of the PM based electromagnetic actuators in case of constant current density [22]. In addition, the gross mass of the actuator is weighed as 174g and it can be derived that the force density of the actuator is approximately 0.014N/g.

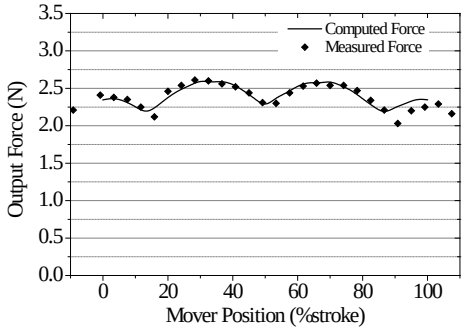


Fig.13 Output force of the large scaled prototype

## 4. Kinetic Modeling of the System

Kinetic performance is one of the important analyses during the design of an actuation system. The analysis can provide elementary kinetic performances of the system including the forces, velocities and displacements. An accurate kinetic model is essential for the analysis of the system. The model can only be developed based on a good understanding of both the electrical and mechanical properties of the system.

### 4.1 Dynamic Modeling of the Linear Actuator

#### 4.1.1 Electrical Equations

The PM linear actuator is the key component of the entire robotic system. The following equation is commonly used for the dynamic analysis of a multi-phase electromagnetic device

$$v_j = r_j i_j + d\lambda_j / dt, \quad j \in (a,b,c), \tag{3}$$

where $v_j$, $i_j$ and $r_j$ are the voltage, current and resistance of the phase $j$, respectively. In order to obtain the dynamic model of the actuator, the flux linkage of the stator windings must be known. Based on the structure of the proposed linear actuator, the flux linkage of each phase can be expressed as

$$\lambda_j = L_{jj} i_j + L_{jk} i_k + L_{jl} i_l + \lambda_{jm}, \ j,k,l \in (a,b,c), \ j \neq k \neq l, \tag{4}$$

where $L_{jj}$ is the self-inductance of each phase, $L_{jk}$, $L_{jl}$ are the mutual inductances between phases, and $\lambda_{jm}$ *is* the magnetizing flux linkage of each phase produced by the PMs. The magnetizing flux linkage

$\lambda_{jm}$ can be found as [23]

$$\lambda_{jm} = \sum_{n=1}^{M} 2\pi r N \int_{z_{j0n}-c_w/2}^{z_{j0n}+c_w/2} B_r(z)dz,\ \ j \in (a,b,c)\,, \tag{5}$$

where $M$ is the number of coil pairs in each phase and $z_{j0n}$ is the center position of each coil pair in the phase. By applying (4) to (3), the electrical equation of the actuator can be obtained as

$$v_j = r_j i_j + d(L_{jj} i_j)/dt + d(L_{jk} i_k)/dt + d(L_{jl} i_l)/dt + e_{jm}\,, \tag{6}$$

where $e_{jm} = d\lambda_{jm}/dt$ is the back electromotive force (EMF) of the phase $j$ generated by the magnetizing flux of PMs. If the saliencies and saturation effect are not considered in the modeling, the inductances will be the constants and (6) can be simplified as

$$v_j = r_j i_j + L_{jj} di_j / dt + L_{jk} di_k / dt + L_{jl} di_l / dt + e_{jm}\,. \tag{7}$$

### 4.1.2 Electromagnetic Force

The electromagnetic force of the actuator can be found by the derivative of the corresponding system co-energy with respect to the displacement, i.e. $F_{em} = \partial W'/\partial z$. According to the electromagnetic field theory, the contributed co-energy of each phase is given by

$$W_j^{'} = \int_0^{i_j} \lambda_j di_j,\ \ j \in (a,b,c)\,. \tag{8}$$

If the saturation effect caused by the stator currents is negligible, the inductances are constants, and (8) can be expressed as

$$W_j^{'} = \tfrac{1}{2} L_{jj} i_j^2 + L_{jk} i_k i_j + L_{jl} i_l i_j + \lambda_{jm} i_j\,. \tag{9}$$

The total co-energy of the actuator is the sum of that of all phases, i.e. $W' = W'_a + W'_b + W'_c$ and the electromagnetic force can then be found as

$$F_{em} = [\partial \Lambda_m / \partial z]^{\mathrm{T}} \cdot I\,, \tag{10}$$

where $\Lambda_m = [\lambda_{am}, \lambda_{bm}, \lambda_{cm}]^{\mathrm{T}}$ and $I = [i_a, i_b, i_c]^{\mathrm{T}}$. The partial differential of the magnetizing flux $\partial\Lambda_m/\partial z$ in (10) can be solved as

$$\partial \Lambda_m / \partial z = 2\pi r N \begin{bmatrix} \sum_{n=1}^{M} \left( B_r(z_{a0n} + c_w/2) - B_r(z_{a0n} - c_w/2) \right) \\ \sum_{n=1}^{M} \left( B_r(z_{b0n} + c_w/2) - B_r(z_{b0n} - c_w/2) \right) \\ \sum_{n=1}^{M} \left( B_r(z_{c0n} + c_w/2) - B_r(z_{c0n} - c_w/2) \right) \end{bmatrix}. \tag{11}$$

### 4.1.3 Dynamic Model of the Actuator

By combining the electrical equations with the electromagnetic force equation, the dynamic model of the proposed linear PM actuator can be achieved as follows

$$\begin{aligned} [dI/dt] &= [L]^{-1}[V - E_m - RI]\,, \\ F_{em} &= [\partial \Lambda_m / \partial z]^{\mathrm{T}} \cdot I \end{aligned} \tag{12}$$

where $V = [v_a, v_b, v_c]^{\mathrm{T}}$, $E_m = [e_{am}, e_{bm}, e_{cm}]^{\mathrm{T}}$, $R = [r_a, r_b, r_c]^{\mathrm{T}}$, and

$$[L]=\begin{bmatrix} L_{aa} & L_{ab} & L_{ac} \\ L_{ba} & L_{bb} & L_{bc} \\ L_{ca} & L_{cb} & L_{cc} \end{bmatrix}.$$

The flux density $B_r$ and the phase inductances required for the model can be obtained from the FE magnetic field analysis of the actuator.

## 4.2 Kinetic Model of the Mobile Robot

### 4.2.1 Kinetic Analysis

According to the structure of the mobile robot, the mechanical model of the system can be schematically illustrated in Fig.14. The forces considered in the mechanical analysis include the electromagnetic force of the linear motor $F_{em}$, the elastic force of the spring $F_{sp}$, the frictional forces of the linear bearings between the stator and mover $F_{bf}$, and the frictional forces between the legs and traveling surface $F_{lg}$. Based on Newton's Law, the kinetic equations of the system can be obtained as

$$\begin{aligned} dv_s / dt &= (-F_{em} + F_{sp} + F_{bfs} + F_{lgs}) / m_s \\ dv_a / dt &= (F_{em} - F_{sp} + F_{bfa} + F_{lga}) / m_a \end{aligned}, \qquad (13)$$

where $m_s$, $m_a$, $v_s$ and $v_a$ are the masses and the velocities of the stator and mover, respectively, and the subscripts *s* and *a* indicate the stator and mover. The elastic force of the spring and the frictional forces of the linear bearings can be determined by Hooke's Law and Coulomb's law of friction.

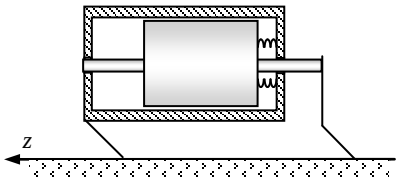


Fig.14 Mechanical model of the system

The frictional force of the bristle-like legs can be analyzed by the following relationship [24]

$$f_{u,v} = \frac{\mu_{m\lg}}{1 \pm \mu_{m\lg} \cot\theta} N_0, \qquad (14)$$

where $N_0$ is the pressing force to the traveling surface, $\mu_{mlg}$ the frictional coefficient between the legs and the surface, and $\theta$ the tilt angle that the legs are mounted to the moving body as shown in Fig.15. The plus sign applies to $f_u$ while the minus sign applies to $f_v$, the subscripts *u* and *v* represent the forward and backward direction, respectively.

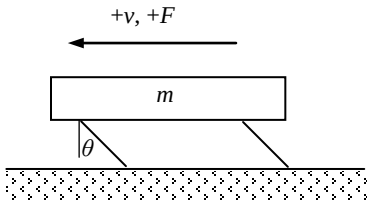


Fig.15 Frictional force of the bristle-like legs

Form (14), it is shown that $f_v$ is always larger than $f_u$. If the angle $\theta$ were selected so that $\mu_{mlg}$ is equal to $\tan\theta$, $f_v$ would be infinity theoretically. In practice, $f_v$ would always counteract the force that makes the actuator move backwards if $\mu_{\mathrm{mlg}}$ is close to $\tan\theta$. As a result, the actuator is automatically locked in the backward direction. Base on this principle, the frictional force $F_{lg}$ can be modeled as

$$F_{\lg x}=\begin{cases}-\dfrac{1}{2}\mu_{mlg}(m_a+m_s)g\cdot sign(v_x)\,, & v_x\geq 0^{+}\\ -\sum F_{others}\,, & v_x=0^{-}\end{cases},\ x=a,s\,. \qquad (15)$$

### 4.2.2 Electro-Mechanical Model of the Robot

By combining the dynamic model of the actuator and the kinetic equations of the mechanical system, the electro-mechanical model of the inchworm mobile robot can be obtained as

$$\begin{aligned}
&[dI/dt]=[L]^{-1}[V-E_m-RI]\\
&dv_s/dt=(-F_{em}+F_{sp}+F_{bfs}+F_{lgs})/m_s\\
&dv_a/dt=(F_{em}-F_{sp}+F_{bfa}+F_{lga})/m_a\ .\\
&dx_s/dt=v_s,\quad v_s\geq 0\\
&dx_a/dt=v_a,\quad v_a\geq 0
\end{aligned} \qquad (16)$$

A performance analysis of the robotic system can be readily conducted by solving the above state equations.

## 5. Actuation Performance Analysis

### 5.1 SIMULINK Model of the Mobile Robot

In order to analyze the actuation performance of the mobile robot, a SIMULINK model of the mobile robot was developed based on the derived electro-mechanical model. Fig.16 shows the block diagram of the model implemented in the SIMULINK environment. The model contains two blocks: the electrical block and the mechanical block. The electrical block solves the electromagnetic force of the actuator and the voltage, current and back EMF in each of the phase based on the input voltages and the relative velocity and position between the stator and mover obtained from the mechanical block. The electromagnetic force is then inputted to the mechanical block along with the other load information to work out the speeds and positions of the stator and mover.

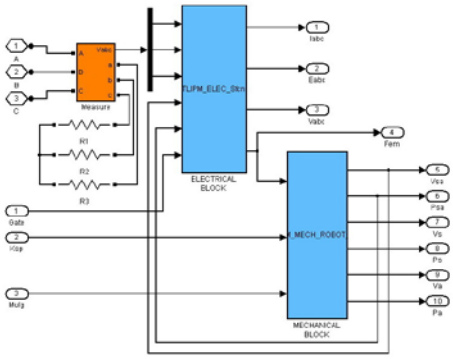


Fig.16 Block diagram of the robotic system model

### 5.2 Sensorless Control Algorithm

The drive control of a PM electrical machine usually requires the position information of the rotor or mover. This can be achieved by either an installed mechanical position sensor or a special designed sensorless algorithm. For the miniature application described in the paper, it is infeasible to install a mechanical position sensor within the actuator due to the restricted space. A sensorless scheme should

be used for the drive control of the linear actuator.

According to the operation of the proposed mobile robot, a sensorless control algorithm with a novel start-up strategy was developed. The scheme utilizes the zero-crossing of the back EMF of the unexcited phase to predict the excitation pattern and the current commutation time. However, it would be difficult to know when the first commutation should be taken place due to the lack of back EMF information at start-up. A commonly used method is applying an open-loop low frequency excitation at the beginning so that the rotor/mover speed could increase high enough to produce the back EMF required for the zero-crossing detection. Nonetheless, it is not applicable for the short stroke linear actuator due to the limited operation distance. Hence, a novel method for the determination of the first commutation was developed by integrating the corresponding back EMF of the actuator. The method is based on the detailed analysis of the profiles of the back EMF in each phase and a criterion is established to decide the time for the current commutation. The method was implemented in SIMULINK environment and the schematic diagram of the control scheme is shown in Fig.17.

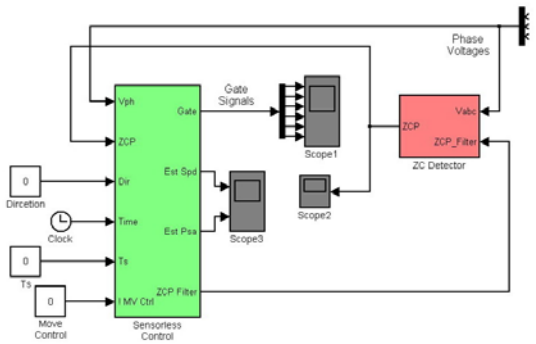


Fig.17 Block diagram of the sensorless control method

In order to achieve the continuous motion behavior, an intermittent drive strategy is integrated with the sensorless control. Since the speed of the mover respected to the stator is estimated in the sensorless control algorithm, the displacement between them can be predicted as well. Accordingly, the drive circuit will be switched off once the displacement reaches the full stroke of the actuator and the force on the mover is removed. Then the stator (main body of the robot) will move forward due to the force of the spring, and an inchworm behavior is achieved by repeating such on-off control strategy.

## 5.3 Performance of the Mobile Robot

The dynamic performance of the entire robotic system was analyzed by applying the drive control system to the electro-mechanical model of the mobile robot. The block diagram of the entire system is illustrated in Fig.18. The power circuit for driving the linear actuator is a three-phase full-bridge inverter made up of low-power semiconductors. All the control units can operate in very low voltages and could be realized by the microelectronic technology and integrated within the mobile robot.

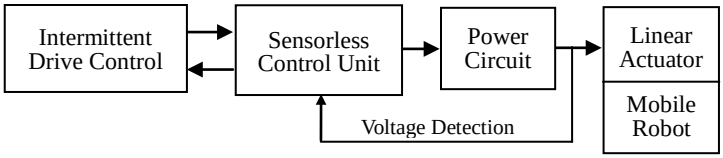


Fig.18 Block diagram of the mobile robot

The simulated actuation performance of the mobile robot is illustrated bellow. The drive frequency for the intermittent motion is about 25Hz. The excitation currents imposed to the actuator are shown in Fig.19 and the electromagnetic force of the actuator during the operation is shown in Fig.20. It can be

seen that the sensorless control algorithm works well with the brushless DC drive scheme and the current commutations are implemented correctly for the appropriate output of the force.

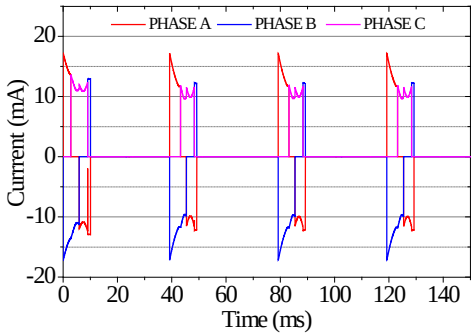


Fig.19 Excitation currents

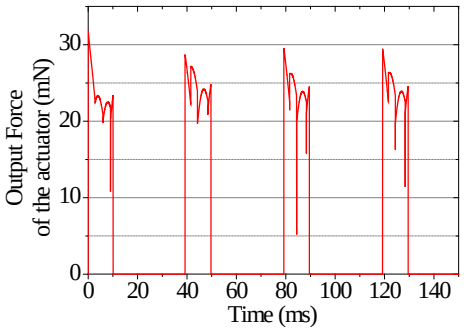


Fig.20 Electromagnetic force of the actuator

The velocities and displacements of the stator and mover are shown in Fig.21. It can be seen that the force of the proposed actuator is satisfactory for the actuation of the robot and the average travel speed of the mobile robot is approximately 45mm/s. In addition, it can be noted from the results that there are collisions taken place when the stator is moving forward while the mover is standstill. The mover acquires speed from the main body and both shift ahead. Therefore, each motion cycle of the robot can be separated into three stages: actuation of the mover, shift of the main body and collision.

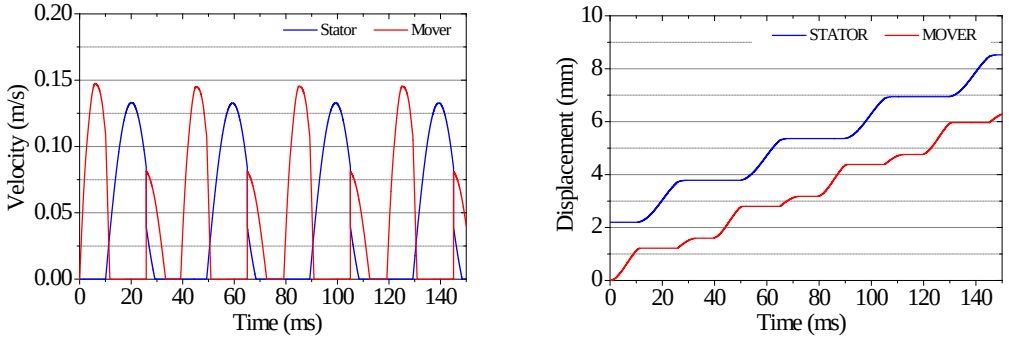


Fig.21 Velocities and displacement of the stator and mover

The energy consumption of the robotic system during the excitation period was also analyzed. During the operation, the average input electric energy of the system is around 12mW and the output mechanical power of the linear actuator is about 2.0mW. Hence, the overall efficiency of the system is about 16%. The rest of the energy is mostly consumed on the resistances of the windings of the actuator. The efficiency of the actuator could be improved by reducing the winding resistances. However, a compromise should be taken in to account between the resistance and the working voltage. Less winding resistances will lead to a very low working voltage that would make it difficult in back EMF detection for the sensorless control scheme.

## 6. Conclusion

The design and analysis of a short stroke electromagnetic linear based inchworm mobile robot is presented. The operation of the robot is accomplished by the bristle-based unidirectional mechanism and the reciprocation of the actuator. The linear actuator is deliberately designed to obtain the optimal force output within a limited space and the experimental verification shows the effectiveness of the proposed actuator. A sensorless control scheme with a novel start-up strategy was developed and analyzed based on the robotic system modeling. The simulated results show the satisfactory performance of the whole system.